



Comparison of Different Spectral Ranges to Monitor Alcoholic and Acetic Fermentation of Red Grape Must Using FT-NIR Spectroscopy and PLS Regression

Camilla Menozzi¹ · Giorgia Foca^{1,2} · Rosalba Calvini^{1,2} · Lisa Catellani³ · Andrea Bezzecchi³ · Alessandro Ulrici^{1,2}

Received: 16 April 2024 / Accepted: 12 May 2024
© The Author(s) 2024

Abstract

Wine vinegar is produced through a two-phase fermentation of grape must: initially, yeast converts grape sugars into ethanol, and subsequently, acetobacteria oxidize ethanol into acetic acid. This process, spanning weeks when conducted by surface fermentation, requires constant monitoring of ethanol and total acidity levels. To enhance the quality and efficiency of process monitoring, vinegar production is shifting to faster, environmentally sustainable methods. Near-infrared (NIR) spectroscopy, recognized for its non-invasiveness and speed, is ideal for online implementation in process control. This study tracked dual fermentation in red grape must over an extended period, monitoring two different batches simultaneously to assess fermentation kinetics and reproducibility. Ethanol content and total acidity were analyzed in fermenting musts throughout the whole fermentation process using both classical laboratory analyses and FT-NIR spectroscopy. Principal Component Analysis (PCA) was used to explore the spectral dataset, then Partial Least Squares (PLS) was used to develop calibration models for predicting ethanol and acidity. The models calculated considering the entire spectral range were compared with those obtained for two narrower zones, where more cost-effective and easily miniaturizable sensors are available on the market. FT-NIR allowed to effectively determine ethanol content and acidity ($R^2_{\text{Pred}} > 0.98$), both over the entire range (12,500–4000 cm^{-1} , corresponding to 800–2500 nm) and in the 10,526–6060 cm^{-1} (950–1650 nm) region. Although less satisfactory, still acceptable results were obtained in the 12,500–9346 cm^{-1} (800–1070 nm) region ($R^2_{\text{Pred}} > 0.81$), confirming the potential for cost-effective devices in real-time fermentation monitoring.

Keywords Near-infrared spectroscopy · Red grape must · Fermentation · Process monitoring · Multivariate calibration

Introduction

Wine vinegar is a food product derived from the dual fermentation of grape must. This process involves two primary phases: initially, yeast transforms the sugars in grapes into ethanol (Cozzolino 2016), and subsequently, acetobacteria bio-oxidize ethanol produced in the first phase into acetic

acid (Bhat et al. 2014). Achieving full completion of this process may span several weeks when the process is conducted through surface fermentation, requiring periodic monitoring to assess fermentation progression and determine the quantities of its byproducts, such as ethanol content and total acidity.

The increasing need for enhanced product quality and efficiency in vinegar production has induced the gradual shift from conventional, destructive analytical methods to faster, more environmentally sustainable alternatives. Vibrational spectroscopies emerge as a compelling choice to continuously monitor the fermentation stage of grape must, ensuring process control and enabling prompt intervention in case of anomalies during fermentation (Gishen et al. 2005). These techniques offer multiple advantages, being rapid and non-invasive, as they necessitate no prior sample preparation.

Among various vibrational spectroscopies, near-infrared (NIR) spectroscopy stands out for its remarkable

✉ Giorgia Foca
giorgia.foca@unimore.it

¹ Dipartimento Di Scienze Della Vita, Università Di Modena E Reggio Emilia, Padiglione Besta, Via Amendola, 2–42122 Reggio Emilia, Italy

² Centro Interdipartimentale BIOGEST-SITEIA, Università Di Modena E Reggio Emilia, Piazzale Europa, 1–42122 Reggio Emilia, Italy

³ Acetaia San Giacomo, Strada Pennella, 1–42017 Novellara (RE), Italy

versatility. It produces reliable results even when utilized by non-specialized personnel to analyze samples containing bonds such as C–H, N–H, and O–H, with the condition that the analyte concentration is at least 0.1% of the total (Burns and Ciurczak 2007). NIR spectroscopy is exceptionally fast, making it suitable for online implementation in process control, contributing to the ease of automating the control system. On the flip side, the application of this technique initially entails a price to pay, namely, the preliminary work on signals to “train” the system to recognize the relevant features in the sample. NIR spectra serve as a sort of fingerprints of the sample that need to be appropriately “interpreted”; this is done using chemometric methods for spectral analysis, which focus on eliminating irrelevant information and interferences and extracting information useful for solving the problem

of interest (Burns and Ciurczak 2007; Ferrari et al. 2011; Foca et al. 2011, 2016; Barbon et al. 2020).

In the literature, numerous works have investigated the processes of alcoholic and acetic fermentation, employing NIR spectroscopy to quantify various analytes indicative of the fermentation stage. Table 1 provides a summary of these articles, highlighting their characteristics. Firstly, some of them specifically focus on the alcoholic fermentation phase (Buratti et al. 2011; Cozzolino et al. 2006; Di Egidio et al. 2010; Frohman and de Orduna Heidinger 2018; Jiménez-Márquez et al. 2016; Kasemsumran et al. 2022; Ouyang et al. 2016; Peng et al. 2016; Ye et al. 2014; Wu et al. 2014), while others concentrate on acetic fermentation (Sedjoah et al. 2021; Chen et al. 2023; González-Sáiz et al. 2008; Phanomsophon et al. 2019; Yano et al. 1997), depending on whether the final product of interest is wine or vinegar,

Table 1 Overview of literature articles addressing the monitoring of alcoholic and acetic fermentation through FT-NIR spectroscopy

Reference	Food matrix	Investigated process	Analytes of interest	Spectral range	Sampling time
Buratti et al. 2011	Red wine	Alcoholic fermentation	Glucose, fructose, ethanol, and glycerol	12,500–3600 cm^{-1}	Up to 20 days
Cozzolino et al. 2006	Red wine	Alcoholic fermentation	None (just spectra time-related changes)	400–2500 nm	Up to 90 days
Di Egidio et al. 2010	Red wine	Alcoholic fermentation	Glucose, fructose, ethanol, total phenolics, total anthocyanins, and total flavonoids	12,500–3600 cm^{-1}	Up to 35 days
Frohman and de Orduna Heidinger 2018	Red wine must	Alcoholic fermentation	Glucose, fructose, total sugars, and ethanol	12,500–4000 cm^{-1}	Not specified (fed-batch fermentation)
Jiménez-Márquez et al. 2016	Model solutions of grape must components and red wine must	Alcoholic fermentation	Ethanol	3 LEDs emitting at 1.20, 1.30 and 1.70 μm	Up to 180 h
Kasemsumran et al. 2022	Pineapple fruit wine	Alcoholic fermentation	Ethanol, total soluble solids, total acidity, and total volatile acids	11,536–3952 cm^{-1}	Up to 10 days
Ouyang et al. 2016	Rice wine	Alcoholic fermentation	Total sugar content, ethanol, and pH	300–1000 nm	Up to 35 days
Peng et al. 2016	Apple wine	Alcoholic fermentation	Alcohol strength and titratable acidity	12,000–4000 cm^{-1}	Up to 10 days
Ye et al. 2014	Apple wine	Alcoholic fermentation	Soluble solid content, pH, total acidity, and total ester content	12,000–4000 cm^{-1}	Not specified
Wu et al. 2014	Chinese rice wine	Alcoholic fermentation	Ethanol and total acid	10,000–4000 cm^{-1}	Up to 20 days
Sedjoah et al. 2021	Mulberry vinegar	Acetic fermentation	Total acids and total polyphenol contents	900–1700 nm	Up to 10 days
Chen et al. 2023	Vinegar	Acetic fermentation	Ethanol and reducing sugar content	900–1700 nm	Up to 2 weeks
González-Sáiz et al. 2008	Onion vinegar	Acetic fermentation	Biomass, ethanol and acetic acid content	1100–2500 nm	Up to 90 h
Phanomsophon et al. 2019	Rice vinegar	Acetic fermentation	Acetic acid and ethanol	12,500–4000 cm^{-1}	Up to 10 days
Yano et al. 1997	Rice vinegar	Acetic fermentation	Acetic acid and ethanol	400–2500 nm	Up to 8 h

respectively. The articles also differ based on the type of substrate involved in fermentation. Indeed, wine and vinegar can be produced not only from grapes but also from rice, apples, or other cereals or fruits—essentially from any vegetable matrix rich in sugars (Jagtap and Bapat 2015; Solieri and Giudici 2009). Additionally, different articles often consider various spectral ranges for NIR analysis, which can have important implications for the performance of the models.

To the best of our knowledge, no study has been conducted so far to track the entire progression of the dual surface fermentation, encompassing both phases over an extended time period. In this work, we monitored the course of simultaneous fermentation for two different batches of red grape must, to assess the reproducibility of the process kinetics when musts from different red grape varieties are kept under the same environmental conditions. Fermentation was monitored by analyzing ethanol content and total acidity for almost four months, evaluating the evolution over time of both parameters.

At the same time, grape must samples were analyzed using FT-NIR spectroscopy over a broad spectral range between 12,500 and 4000 cm^{-1} . The resulting spectra, after appropriate preprocessing, were initially explored by Principal Component Analysis (PCA, Bro and Smilde 2014), to visualize in the principal components space how they evolved in the different phases of fermentation.

Subsequently, multivariate calibration models were developed and validated to predict ethanol content and total acidity using Partial Least Squares (PLS, Geladi and Kowalski 1986). Firstly, a PLS model was calculated considering the entire spectral range (12,500–4000 cm^{-1} , equivalent to 800–2500 nm). Then, the feasibility of achieving satisfactory calibration models using narrower spectral regions was also investigated, since this could allow the use of cheaper and miniaturizable sensors with potential applications in portable devices. Specifically, we focused on two spectral regions labeled for simplicity as “NIR1” and “NIR2” covering the ranges 10,526–6060 cm^{-1} (950–1650 nm) and 12,500–9346 cm^{-1} (800–1070 nm), respectively. The choice to shorten the spectra to obtain the corresponding signals in these spectral regions is driven by the need to simulate spectra acquired with commercially available devices working in these spectral ranges. The NIR1 region corresponds to the spectral range that could be acquired using an uncooled InGaAs detector, which is significantly more economical than its cooled counterpart. On the other hand, the NIR2 region is towards the NIR region closer to the visible one, which could also allow the use of much cheaper silicon detectors (Wang et al. 2020; Pu et al. 2021).

Monitoring of alcoholic and acetic fermentation in red grape musts through FT-NIR has proven effective in accurately determining ethanol content and total acidity values both considering the entire spectral range and focusing on

the region labeled as NIR1. Less satisfactory but still acceptable results were obtained in the region referred to as NIR2, confirming the potential use of simple and cost-effective devices for real-time monitoring of fermenting must.

Materials and Methods

Must Samples and Fermentation Conditions

In this study, two samples of red grape must, referred to as batch A and batch B, both produced in the agricultural year 2022 in Emilia Romagna Region, Italy, were subjected to surface fermentation. Batch A must was from *Ancelotta* grape variety, while batch B must was from a blend of *Lambrusco Salamino* and *Lambrusco Grasparossa* grape varieties.

After pressing the grapes, the grape musts were cooled and stabilized at a temperature between 0 and 4 °C. Subsequently, as the experimentation began, they were brought to room temperature (ranging from 18 to 25 °C during the whole fermentation period) and inoculated with *Saccharomyces cerevisiae* yeast to initiate the alcoholic fermentation process. Throughout the alcoholic fermentation phase, two aliquots of grape must were collected almost daily for each batch. One was promptly analyzed in the laboratory to determine ethanol content and total acidity, while the other was frozen for subsequent spectroscopic analysis. Starting around the 40th day of fermentation, the acetic bio-oxidation phase began spontaneously (acetobacteria were present in the air of the fermentation room, which is adjacent to a vinegar production area). During this phase, sampling of the two aliquots for each batch was conducted every 2–4 days. In total, 49 samples were collected for batch A and 40 samples for batch B, for which the fermentation process proceeded more rapidly. Monitoring ended after 116 days for batch A and after 80 days for batch B.

Laboratory Analysis and Spectra Acquisition

Each sampling day, ethanol content (% v/v) was measured in triplicate using a Malligand ebulliometer (Ing. Bullio Castore, Milan, Italy). Total acidity (g/100 ml) was also measured in triplicate utilizing a potentiometric titrator (TitraLab AT1000, Hach-Crison, Barcelona, Spain). Additionally, at the time of aliquot collection, the temperature of the musts was recorded with a food thermometer (Tecna2, Tecnafood, Bomporto, Italy) to track the trend and identify potential fermentation anomalies.

Regarding spectroscopic analysis, after some preliminary tests, an appropriate sample treatment and signal acquisition procedure was developed. The aliquots of frozen must intended for analysis were transferred from the freezer to

the refrigerator the evening before the analysis day to ensure complete thawing of the sample without restarting fermentation. Thirty minutes prior to analysis, the samples were extracted from the refrigerator and filtered through a 25- μm cellulose filter to eliminate suspended particles.

Fourier-transform near-infrared (FT-NIR) spectra were acquired in transmission mode using a Bruker Multi Purpose Analyzer (MPA) spectrophotometer equipped with a TE-InGaAs sensor, that is thermoelectrically cooled to ensure a high signal-to-noise ratio (Beć et al. 2022). Measurements were performed using a quartz Suprasil cuvette with an optical path length of 0.5 mm. A background spectrum was acquired on the empty cuvette before the analysis of each aliquot. To evaluate measurement repeatability and enhance the robustness of calibration models, three spectra were acquired for each sample, corresponding to three distinct sample aliquots. Each spectrum, derived from the average of 128 scans, was collected throughout the entire spectral range (12,500–4000 cm^{-1}) excluding the low-wavenumber region between 4000 and 3600 cm^{-1} where the signal was too noisy. Considering a spectral resolution of 4 cm^{-1} , each spectrum was composed of a total of 4407 variables. Given that it is well-known from the literature that temperature variation causes changes in both the position and intensity of bands in the NIR spectrum, especially for aqueous and alcoholic samples (Cozzolino et al. 2007; Wulfert et al. 1998), the cuvette compartment was maintained at a constant temperature of 28 °C during measurements. This was implemented to mitigate any potential variability associated with differences in the laboratory's ambient temperature throughout the entire period during which NIR analyses were conducted.

Data Analysis

The spectral dataset, including 267 spectra, i.e., (49 samples from batch A + 40 samples from batch B) \times 3 replicates, was first subjected to exploratory data analysis using Principal Component Analysis (PCA). This analysis aimed to evaluate the reproducibility of measurements, potential variations between samples from different batches, identification of outliers, and exploration of trends related to ethanol content and total acidity. Based on some preliminary tests, spectra were preprocessed using Standard Normal Variate (SNV) and mean centering.

Subsequently, Partial Least Squares (PLS) was employed as a multivariate calibration method to determine the values of ethanol and acidity from NIR spectra. The calibration models were initially derived from full NIR spectra, encompassing a spectral range spanning the entire acquired region (12,500–4000 cm^{-1}). Analogous PLS models were also developed for two additional spectral datasets, obtained by trimming the signals to keep only specific spectral ranges. In detail, the dataset abbreviated as NIR1 encompasses the

spectral range from 10,526 to 6060 cm^{-1} (equivalent to 950–1650 nm), while the dataset referred to as NIR2 covers the range from 12,500 to 9346 cm^{-1} (corresponding to 800–1070 nm).

To calculate all the PLS models, the spectral datasets were randomly divided into a calibration set (training set) containing 180 spectra (60 samples \times 3 replicates) and an external validation set (test set) containing the remaining 87 spectra (29 samples \times 3 replicates). Based on some preliminary trials conducted on the training set, the optimal spectral preprocessing for predicting the parameters of interest resulted from a combination of smoothing (first-order, 15 points window), SNV, and mean centering. The optimal number of latent variables (LVs) was chosen by minimizing the cross-validation error that was estimated using a venetian blinds procedure with 10 deletion groups, each including 18 spectra (corresponding to the 3 replicates of 6 samples). Subsequently, the models were validated using the external test set.

The performance of the calibration models was evaluated using Root Mean Square Error (RMSE) and coefficient of determination (R^2) metrics. These metrics were calculated on the training set for calibration (RMSEC, R^2_{Cal}) and cross-validation (RMSECV, R^2_{CV}) and then on the test set for validation (RMSEP, R^2_{Pred}).

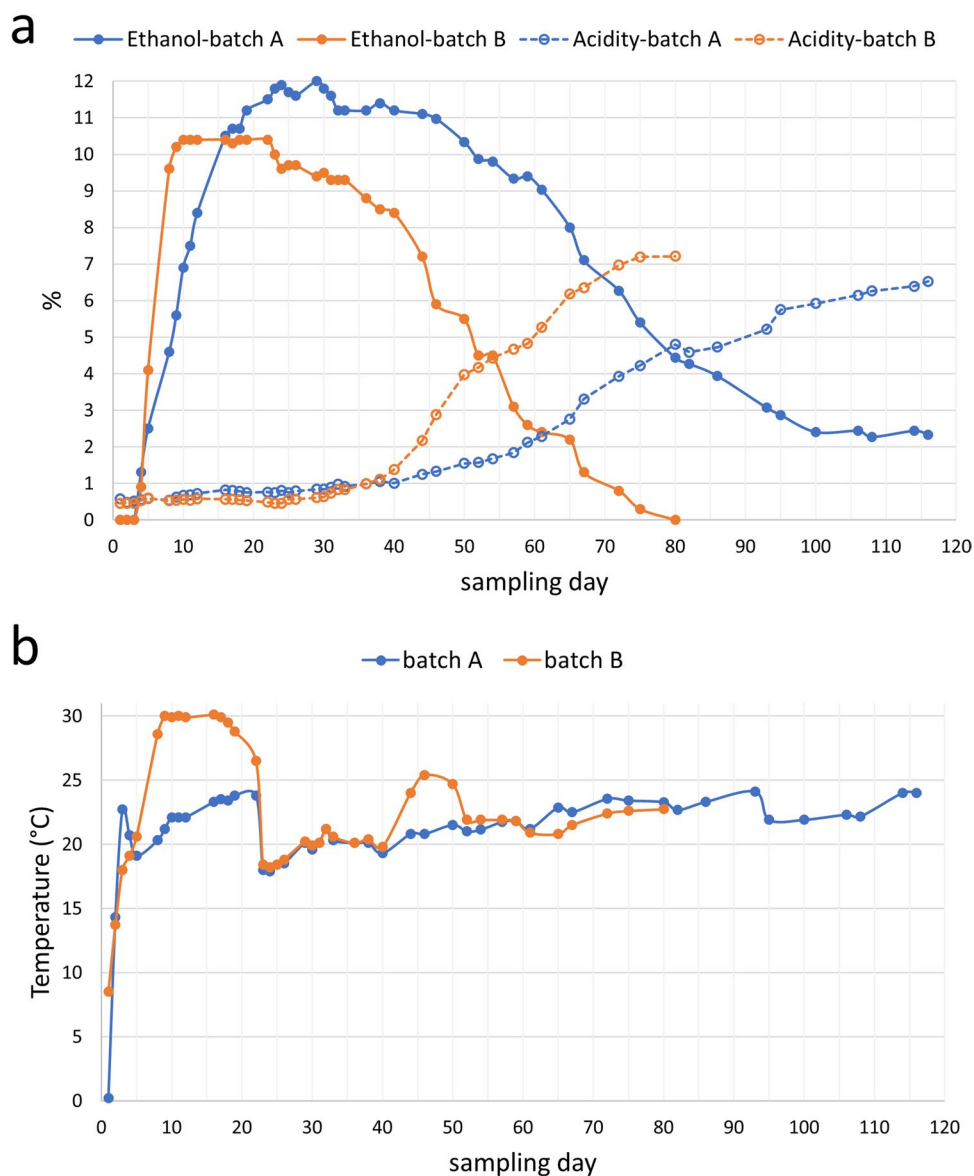
The PLS models were calculated using the PLS Toolbox (version 8.8.1, Eigenvector Research Inc., USA) operating in the MATLAB environment (version 2022b, The Mathworks Inc., USA).

Results and Discussion

Exploratory Analysis of Laboratory Parameters

The laboratory-measured physicochemical parameters (ethanol content, total acidity, and temperature) were plotted to evaluate their trends over time for the two batches. Figure 1a illustrates the variation in ethanol content and total acidity with respect to fermentation time, where each reported value is the average of three replicate measurements. From the graph, it can be observed that the ethanol content and total acidity values followed a similar pattern in both batches, but each batch progressed at a different rate. Initially, a rapid increase in ethanol content was observed, reaching its peak around day 10 for batch B and around day 25 for batch A. Around day 40, total acidity started to increase, while alcohol content declined rapidly. For batch B, ethanol was depleted after 80 days, leading to the end of fermentation. In the case of batch A, the formation of acetic acid continued more gradually, and at the time of sampling interruption, ethanol was not yet fully depleted.

Fig. 1 Variation in ethanol content and total acidity (a) and temperature (b) on different sampling days during the fermentation period



For thoroughness, the graph illustrating the temperature changes over time is included as well (Fig. 1b). Temperature demonstrated a more stable pattern for batch A, whereas it exhibited two distinct peaks for batch B. Specifically, for batch B, temperature reached around 30 °C at the peak of alcoholic fermentation, then decreased and slightly increased again at the onset of acetic oxidation.

Exploratory Analysis of FT-NIR Spectra

Figure 2 reports the score plots of the first two principal components (PCs) of the PCA model calculated on the whole dataset of FT-NIR spectra, accounting for 91.20% of total data variance. In Fig. 2a, where the samples are color-coded by batch, it is observed that the spectra belonging to the two batches are distinguishable in the PC

space, although the fermentation evolution essentially follows the same trend for both musts. This analogy becomes more evident when the samples are colored based on the sampling day, as reported in Fig. 2b. Up to approximately day 40, the values of PC1 remain approximately constant, while the values of PC2 decrease. Then, the values of PC1 gradually increase, while the values of PC2 show a less pronounced rise.

In Fig. 2c, d, the same score plot is depicted based on ethanol content and total acidity values, respectively. Figure 2c shows that, during alcoholic fermentation, the PC2 values gradually decrease while the PC1 values remain relatively constant. Subsequently, as acetic oxidation begins, the PC1 value progressively rises (Fig. 2d) in tandem with the gradual consumption of ethanol (Fig. 2c). Therefore, samples with high acidity exhibit high PC1 values, while

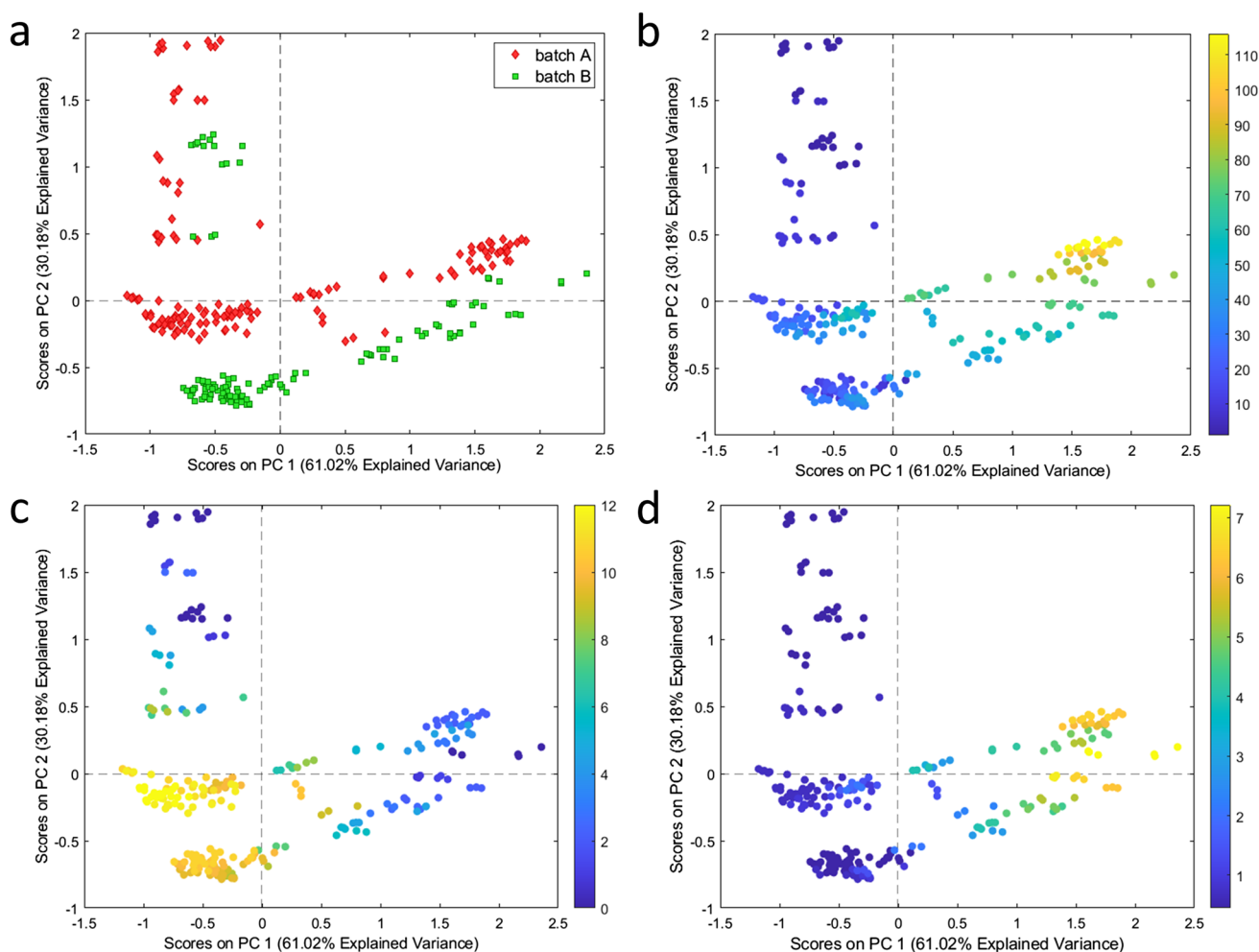


Fig. 2 Score plots of PC1 vs PC2 of the PCA model obtained on the complete FT-NIR spectral dataset. Samples are colored based on batch (**a**), on fermentation day (**b**), on ethanol content (**c**), and on total acidity (**d**)

samples with high ethanol content have low values for both PC1 and PC2.

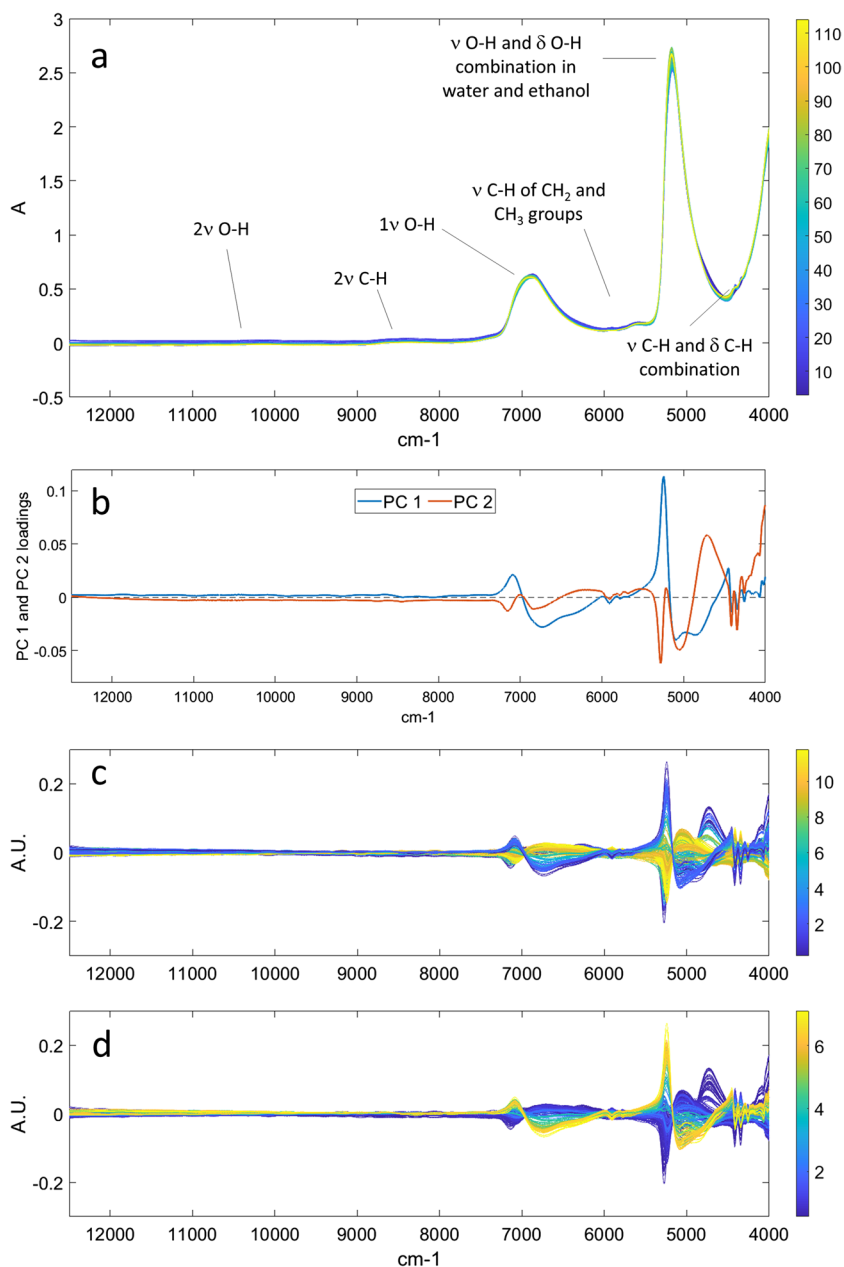
Through the loading plots, it is possible to analyze the contribution of each spectral variable to the two PCs of the model and identify correlations. In Fig. 3a, the original spectra are colored based on the fermentation day, along with indications of the attributions of the main spectral bands according to the literature (Nespeca et al. 2017; Dong et al. 2019; Cozzolino et al. 2006; Di Egidio et al. 2010; Kasemsumran et al. 2022; Ye et al. 2014). In Fig. 3b, the loading plots of PC1 and PC2 are reported, in comparison with the preprocessed spectra, colored based on both ethanol content (Fig. 3c) and total acidity (Fig. 3d). Firstly, it can be observed that from the raw spectra (Fig. 3a), it is not possible to clearly discern any trend with fermentation time, as the signals are highly overlapped and exhibit a very similar profile. However, the subsequent application of preprocessing highlights the differences (Fig. 3c, d).

According to existing literature, it is well-established that the absorption pattern in the NIR region during the

fermentation of grape must is predominantly influenced by the water spectrum (Jiménez-Márquez et al. 2016). The presence of water gives rise to intense and broad bands attributed to the O–H bend stretching and the combination of O–H stretching and bending, as illustrated in Fig. 3a. However, it is worth noting that ethanol and acetic acid absorb at approximately the same wavelengths, as these molecules partially share similar chemical bonds and functional groups, just like fructose, glucose, and glycerol always present in grape musts. Therefore, any differences in the spectra of samples at different fermentation stages can be attributed to subtle variations in the relative intensity of peaks and/or to the horizontal shift of these peaks due to their chemical surroundings.

Nonetheless, it is interesting to observe how the two adjacent peaks at around $4400\text{--}4300\text{ cm}^{-1}$ increase with the rise in alcohol percentage, while the loadings of PC2 decrease in this region, aligning with the patterns seen in the score plot of Fig. 2c. These peaks are distinctive of ethanol, attributed to the combination band of C–H in the $-\text{CH}_2$ and

Fig. 3 Original spectra colored according to the fermentation day with assignment of the main spectral bands (a) compared to the loadings plots of PC1 and PC2 (b) and with preprocessed spectra colored based on ethanol content (c) and total acidity (d)



-CH₃ groups (Dong et al. 2019; Cozzolino et al. 2006; Di Egidio et al. 2010). Conversely, the spectral variables that appear more correlated with acetic acid content (Fig. 3d) are those associated with the peak at approximately 5170 cm⁻¹,

linked to the combination of O–H stretching and bending vibrations. In addition to increasing in intensity (like the loadings of PC1), it undergoes a slight shift towards higher wavenumbers (Cozzolino et al. 2006; Di Egidio et al. 2010).

Table 2 Performance of PLS models obtained for ethanol content and total acidity considering the three spectral ranges

Spectral range	Y	#LVs	RMSEC	RMSECV	RMSEP	R ² _{Cal}	R ² _{CV}	R ² _{Pred}
Complete	Ethanol	5	0.399	0.435	0.412	0.990	0.988	0.990
	Acidity	6	0.114	0.135	0.218	0.997	0.996	0.990
NIR1	Ethanol	5	0.427	0.469	0.463	0.989	0.986	0.987
	Acidity	8	0.147	0.169	0.196	0.995	0.994	0.992
NIR2	Ethanol	8	1.625	1.981	1.561	0.834	0.755	0.849
	Acidity	5	0.907	1.040	0.909	0.818	0.762	0.813

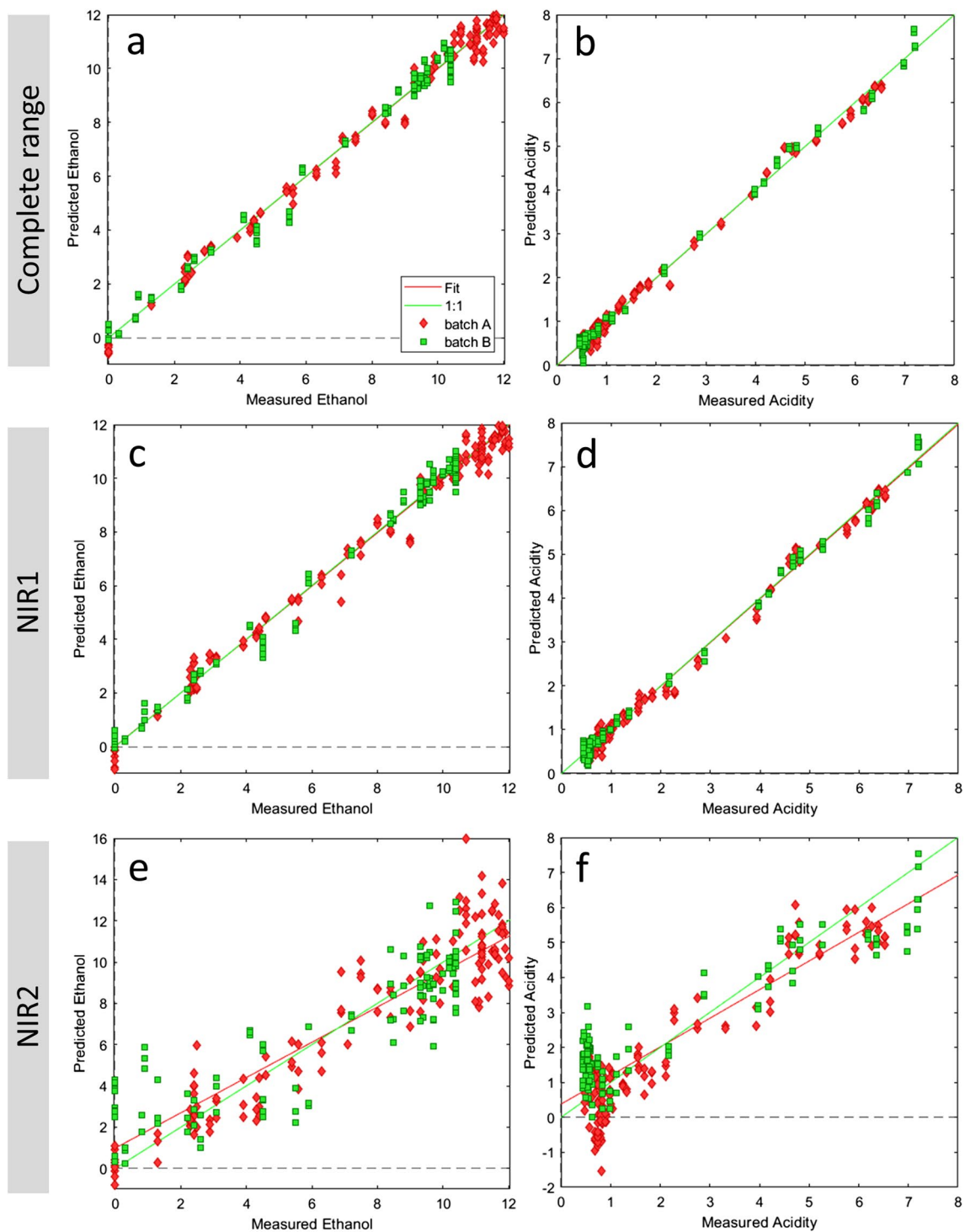


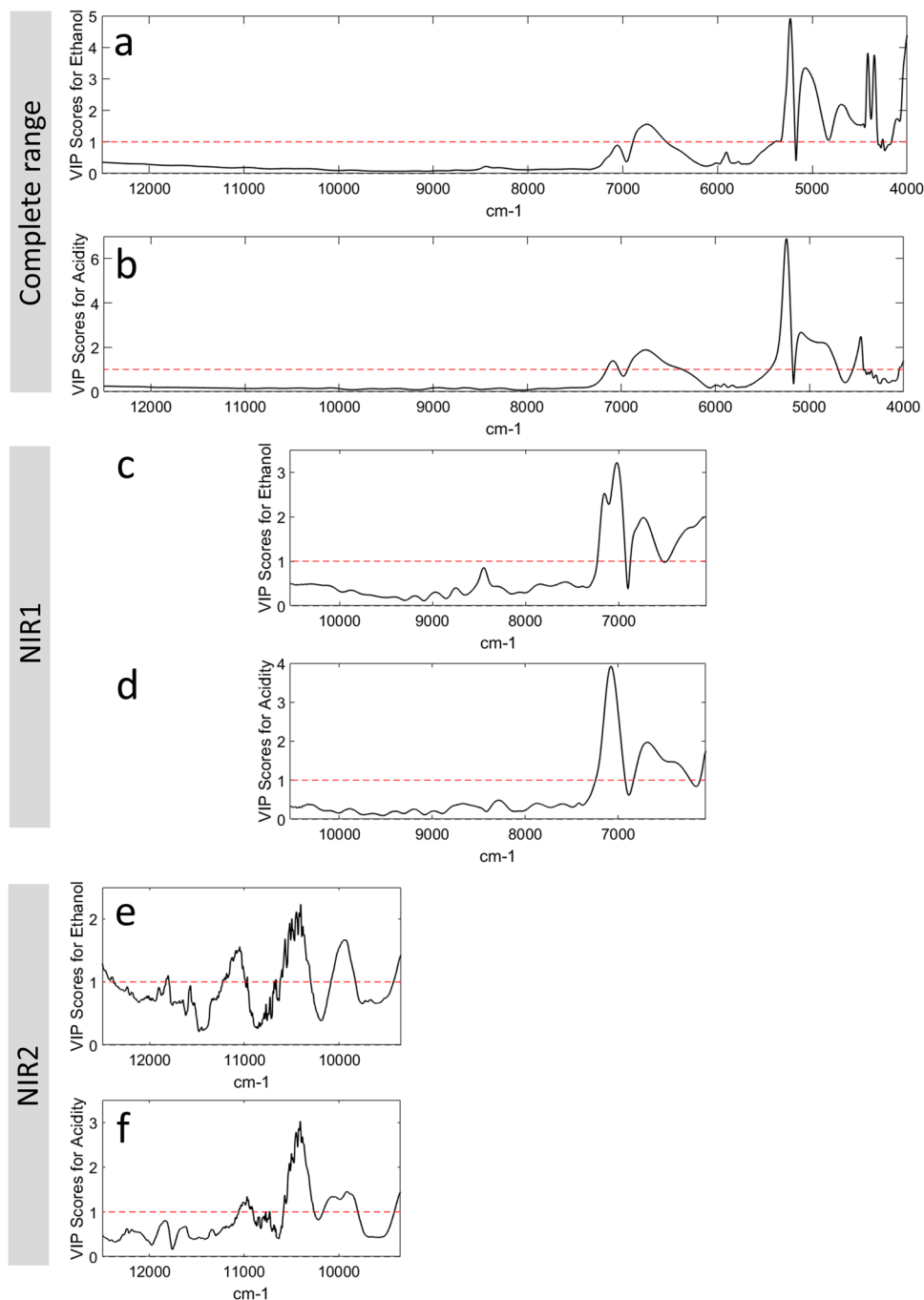
Fig. 4 Y measured vs. Y predicted plots of PLS models obtained on the complete spectra for ethanol content (a) and total acidity (b), on the NIR1 region for ethanol content (c) and total acidity (d), and for the NIR2 region for ethanol content (e) and total acidity (f)

Calibration

As detailed in the “Data Analysis” section, calibration models were developed for three distinct datasets: the complete NIR spectra dataset ($12,500\text{--}4000\text{ cm}^{-1}$), the

dataset labeled as NIR1 ($10,526\text{--}6060\text{ cm}^{-1}$), and the dataset labeled as NIR2, which includes only the spectral region adjacent to the visible range ($12,500\text{--}9346\text{ cm}^{-1}$). In each case, the same sample partitioning into training set, test set, and deletion groups for cross-validation was

Fig. 5 VIP score plots of PLS models obtained on the complete spectra for ethanol content (a) and total acidity (b), on the NIR1 region for ethanol content (c) and total acidity (d), and for the NIR2 region for ethanol content (e) and total acidity (f)



used, along with identical signal preprocessing. This ensured complete comparability of the models.

Table 2 provides a comparison of the performance of all the obtained calibration models. It is worth noting that excellent models were achieved for both parameters when considering both the complete spectrum and the NIR1 region, with R^2_{Pred} values exceeding 0.98 in each case. However, performance in the NIR2 region is notably less satisfactory, albeit still of acceptable quality for screening

analysis aimed at providing indicative results on ethanol and acidity content in grape musts.

Figure 4 reports the laboratory-measured parameter values against the values predicted by the FT-NIR models for the three spectral regions and the two investigated properties. Consistently with the model performance parameters outlined in Table 2, the measured values closely align with the predicted values for both the complete spectrum and the NIR1 region (Fig. 4a–d). On the contrary, in the graphs regarding the NIR2

region (Fig. 4e, f), a higher dispersion of samples around the fitted line (represented in red) is observed; furthermore, the bisector (represented in green) and the fitted line do not overlap, in contrast to the earlier models. Specifically, for batch B samples, both models predict ethanol content and total acidity values higher than the actual values at low levels of these parameters; for batch A, the total acidity model predicts lower values than the actual ones at low total acidity levels.

Finally, in Fig. 5, the Variable Importance in Projections (VIP) scores of the models are presented. The spectral variables positioned above the threshold value set equal to 1 (red dashed line) in the VIP plots are the most valuable for modeling ethanol content and acidity (Gosselin et al. 2010). It is evident that, for the complete spectrum, the VIP scores of the ethanol content model (Fig. 5a) differ from those of the acidity model (Fig. 5b), especially in the region of the two adjacent peaks at around 4400–4300 cm^{-1} . As mentioned earlier, these peaks are characteristic of ethanol (C–H combination bands in the $-\text{CH}_2$ and $-\text{CH}_3$ groups). Crucial for constructing both models are the spectral variables associated with the combination of O–H stretching and bending vibrations (around 5170 cm^{-1}) and the stretching of the O–H bond (around 7000–6800 cm^{-1}).

For the models calculated considering the NIR1 region (Fig. 5c, d), there is a slight alteration in the VIP scores graphs, given that these models cannot benefit from the information of bands below 6000 cm^{-1} . Consequently, the significant variables primarily involve the stretching of the O–H bond, a functional group found in both ethanol and acetic acid, as well as in the predominant aqueous matrix. Comparing the VIP scores with the shape of the original signals in Fig. 3a, it emerges that, during fermentation, this peak decreases in intensity and gradually shifts towards higher wavenumbers.

For the models in the NIR2 region, the presence of noise due to the low signal-to-noise ratio in this spectral region is immediately noticeable. However, the application of smoothing preprocessing has partially mitigated this issue. Additionally, from the VIP plots, it is observed how some spectral variables, not considered fundamental in the previous models, have now become significant. Specifically, the graphs suggest that the peak where the most pertinent information for the models is concentrated lies at approximately 10,300 cm^{-1} , corresponding to the second overtone of the O–H stretching vibration (Jiménez-Márquez et al. 2016).

Conclusions

The aim of this study was to test the effectiveness of NIR spectroscopy to monitor the surface fermentation process of red grape must, comparing the results that could be obtained

with devices operating in different NIR spectral regions. To this aim, we conducted a simultaneous analysis of two different batches of red grape must undergoing fermentation over an extended period up to about 4 months. During this time, the musts were subjected to both alcoholic and acetic fermentation stages.

In particular, our goal was to simulate the use of devices operating in different spectral regions to assess the potential of various commercial instruments. Specifically, models were generated over the entire range from 12,500 to 4000 cm^{-1} , corresponding to expensive benchtop instruments, in the 10,526–6060 cm^{-1} range, corresponding to high-end portable instruments, and in the 12,500–9346 cm^{-1} range, corresponding to economical handheld instruments.

Overall, the results were excellent for models obtained considering the entire spectrum and the 10,526–6060 cm^{-1} region. Results obtained for the 12,500–9346 cm^{-1} region were less satisfactory but still acceptable for fast screening. This indicates that FT-NIR spectroscopy, even in its simpler and more economical versions, remains an optimal choice for product monitoring in the field of vinegar production, as it combines speed and efficiency with the non-invasiveness of the analysis, preserving the integrity of the sample.

Acknowledgements The authors sincerely thank Beatrice Guzzi and Paolo Tucci of Acetyca s.r.l. (Saronno, Italy) for their generous support and collaboration. Rosalba Calvini would like to thank the Italian funding program Fondo Sociale Europeo REACT-EU-PON “Ricerca e Innovazione” 2014–2020–Azione IV.6 Contratti di ricerca su tematiche Green (D.M. 1062 del 10/08/ 2021) for supporting her research (CUP: E95F21002330001; contract number 17-G-13884–4).

Author Contribution C. Menozzi: investigation, methodology, formal analysis, and writing—original draft. G. Foca: conceptualization, methodology, formal analysis, and writing—original draft. R. Calvini: methodology, formal analysis, and writing—review and editing. L. Catelani: investigation, methodology, and writing—review and editing. A. Bezecchi: supervision, conceptualization, and writing—review and editing. A. Ulrici: supervision, project administration, conceptualization, and writing—review and editing.

Funding Open access funding provided by Università degli Studi di Modena e Reggio Emilia within the CRUI-CARE Agreement. The project was supported by Acetyca S.r.l. (Saronno, Italy).

Data Availability No datasets were generated or analyzed during the current study.

Declarations

Competing Interests The authors declare no competing interests.

Open Access This article is licensed under a Creative Commons Attribution 4.0 International License, which permits use, sharing, adaptation, distribution and reproduction in any medium or format, as long as you give appropriate credit to the original author(s) and the source, provide a link to the Creative Commons licence, and indicate if changes were made. The images or other third party material in this article are

included in the article's Creative Commons licence, unless indicated otherwise in a credit line to the material. If material is not included in the article's Creative Commons licence and your intended use is not permitted by statutory regulation or exceeds the permitted use, you will need to obtain permission directly from the copyright holder. To view a copy of this licence, visit <http://creativecommons.org/licenses/by/4.0/>.

References

- Barbon SJ, Mastelini SM, Barbon APAC, Barbin DF, Calvini R, Lopes JF, Ulrici A (2020) Multi-target prediction of wheat flour quality parameters with near infrared spectroscopy. *Inf Process Agric* 7:342–354. <https://doi.org/10.1016/j.inpa.2019.07.001>
- Beć KB, Grabska J, Huck CW (2022) Miniaturized NIR spectroscopy in food analysis and quality control: promises, challenges, and perspectives. *Foods* 11:1465. <https://doi.org/10.3390/foods11101465>
- Bhat SV, Akhtar R, Amin T (2014) An overview on the biological production of vinegar. *Int J Fermented Foods* 3(2):139–155. <https://doi.org/10.5958/2321-712X.2014.01315.5>
- Bro R, Smilde AK (2014) Principal component analysis. *Anal. Methods* 6:2812–2831. <https://doi.org/10.1039/C3AY41907J>
- Buratti S, Ballabio D, Giovanelli G, Zuluanga Dominguez CM, Moles A, Benedetti S, Sinelli N (2011) Monitoring of alcoholic fermentation using near infrared and mid infrared spectroscopies combined with electronic nose and electronic tongue. *Anal Chim Acta* 697:67–74. <https://doi.org/10.1016/j.aca.2011.04.020>
- Burns DA, Ciurczak EW (2007) *Handbook of near-infrared analysis – 3rd Edition*. CRC Press, pp. ix–x. <https://doi.org/10.1201/9781420007374>
- Chen C, Li X, Zhu S, Cui P, Lei H, Yan H (2023) Detection of the alcohol fermentation process in vinegar production with a digital micro-mirror based NIR spectra set-up and chemometrics. *J Food Compost Anal* 115:105036. <https://doi.org/10.1016/j.jfca.2022.105036>
- Cozzolino D (2016) State-of-the-art advantages and drawbacks on the application of vibrational spectroscopy to monitor alcoholic fermentation (beer and wine). *Appl Spectrosc Rev* 51(4):282–297. <https://doi.org/10.1080/05704928.2015.1132721>
- Cozzolino D, Parker M, Damberg RG, Herderich M, Gishen M (2006) Chemometrics and visible-near infrared spectroscopic monitoring of red wine fermentation in a pilot scale. *Biotechnol Bioeng* 95(6):1101–1107. <https://doi.org/10.1002/bit.21067>
- Cozzolino D, Liua L, Cynkar WU, Damberg RG, Janik L, Colby CB, Gishen M (2007) Effect of temperature variation on the visible and near infrared spectra of wine and the consequences on the partial least square calibrations developed to measure chemical composition. *Anal Chim Acta* 588:224–230. <https://doi.org/10.1016/j.aca.2007.01.079>
- Di Egidio V, Sinelli N, Giovanelli G, Moles A, Casiraghi E (2010) NIR and MIR spectroscopy as rapid methods to monitor red wine fermentation. *Eur Food Res Technol* 230:947–955. <https://doi.org/10.1007/s00217-010-1227-5>
- Dong Q, Yu C, Li L, Nie L, Li D, Zang H (2019) Near-infrared spectroscopic study of molecular interaction in ethanol-water mixtures. *Spectrochim Acta A Mol Biomol Spectrosc* 222:117183. <https://doi.org/10.1016/j.saa.2019.117183>
- Ferrari E, Foca G, Vignali M, Tassi L, Ulrici A (2011) Adulteration of the anthocyanin content of red wines: perspectives for authentication by Fourier Transform-Near InfraRed and ¹H NMR spectroscopies. *Anal Chim Acta* 701(2):139–151. <https://doi.org/10.1016/j.aca.2011.05.053>
- Foca G, Ferrari C, Sinelli N, Mariotti M, Lucisano M, Caramanico R, Ulrici A (2011) Minimisation of instrumental noise in the acquisition of FT-NIR spectra of bread wheat using experimental design and signal processing techniques. *Anal Bioanal Chem* 399(6):1965–1973. <https://doi.org/10.1007/s00216-010-4431-z>
- Foca G, Ferrari C, Ulrici A, Ielo MC, Minelli G, Lo Fiego DP (2016) Iodine value and fatty acids determination on pig fat samples by FT-NIR spectroscopy: benefits of variable selection in the perspective of industrial applications. *Food Anal Methods* 9(10):2791–2806. <https://doi.org/10.1007/s12161-016-0478-6>
- Frohman CA, de Orduña Mira, Heidinger R (2018) The substratostat an automated near-infrared spectroscopy-based variable-feed system for fed-batch fermentations of grape musts. *OENO One* 52(4):279–289. <https://doi.org/10.20870/oeno-one.2018.52.4.2199>
- Geladi P, Kowalski BR (1986) Partial least-squares regression: a tutorial. *Anal Chim Acta* 185:1–17. [https://doi.org/10.1016/0003-2670\(86\)80028-9](https://doi.org/10.1016/0003-2670(86)80028-9)
- Gishen M, Damberg RG, Cozzolino D (2005) Grape and wine analysis – enhancing the power of spectroscopy with chemometrics. A review of some applications in the Australian wine industry. *Aust J Grape Wine Res* 11:296–305. <https://doi.org/10.1111/j.1755-0238.2005.tb00029.x>
- González-Sáiz JM, Esteban-Díez I, Sánchez-Gallardo C, Pizarro C (2008) Monitoring of substrate and product concentrations in acetic fermentation processes for onion vinegar production by NIR spectroscopy: value addition to worthless onions. *Anal Bioanal Chem* 391:2937–2947. <https://doi.org/10.1007/s00216-008-2186-6>
- Gosselin R, Rodrigue D, Duchesne C (2010) A Bootstrap-VIP approach for selecting wavelength intervals in spectral imaging applications. *Chemom Intel Lab Syst* 100(1):12–21. <https://doi.org/10.1016/j.chemolab.2009.09.005>
- Jagtap UB, Bapat VA (2015) Wines from fruits other than grapes: current status and future prospectus. *Food Biosci* 9:80–96. <https://doi.org/10.1016/j.fbio.2014.12.002>
- Jiménez-Márquez F, Vázquez J, Úbeda J, Sánchez-Rojas JL (2016) Optoelectronic sensor for measuring ethanol content during grape must fermentation using NIR spectroscopy. *Microsyst Technol* 22:1799–1809. <https://doi.org/10.1007/s00542-016-2835-1>
- Kasemsumran S, Boondaeng A, Ngowsuwan K, Jungtheerapanich S, Apiwatanapiwat W, Janchai P, Meelaksana J, Vaithanomsat P (2022) Simultaneous monitoring of the evolution of chemical parameters in the fermentation process of pineapple fruit wine using the liquid probe for near-infrared coupled with chemometrics. *Foods* 11:377. <https://doi.org/10.3390/foods11030377>
- Nespeca MG, Varella Rodrigues C, Oliveira Santana K, Maintinguer SI, de Oliveira JE (2017) Determination of alcohols and volatile organic acids in anaerobic bioreactors for H₂ production by near infrared spectroscopy. *Int J Hydrogen Energy* 42:20480–20493. <https://doi.org/10.1016/j.ijhydene.2017.07.044>
- Ouyang Q, Zhao J, Pan W, Chen Q (2016) Real-time monitoring of process parameters in rice wine fermentation by a portable spectral analytical system combined with multivariate analysis. *Food Chem* 190:135–141. <https://doi.org/10.1016/j.foodchem.2015.05.074>
- Peng B, Ge N, Cui L, Zhao H (2016) Monitoring of alcohol strength and titratable acidity of apple wine during fermentation using near-infrared spectroscopy. *LWT Food Sci Technol* 66:86–92. <https://doi.org/10.1016/j.lwt.2015.10.018>
- Phanomsoophon T, Sirisomboon P, Lapcharoensuk R, Shrestha B, Krusong W (2019) Evaluation of acetic acid and ethanol concentration in a rice vinegar internal venturi injector bioreactor using Fourier transform near infrared spectroscopy. *J Near Infrared Spectrosc* 27(6):096703351987030. <https://doi.org/10.1177/0967033519870304>
- Pu Y, Pérez-Marín D, O'Shea N, Garrido-Varo A (2021) Recent advances in portable and handheld NIR spectrometers and

- applications in milk, cheese and dairy powders. *Foods* 10:2377. <https://doi.org/10.3390/foods10102377>
- Sedjoah RCAA, Maa Y, Xiong M, Yan H (2021) Fast monitoring total acids and total polyphenol contents in fermentation broth of mulberry vinegar using MEMS and optical fiber near-infrared spectrometers. *Spectrochim Acta A Mol Biomol Spectrosc* 260:119938. <https://doi.org/10.1016/j.saa.2021.119938>
- Solieri L, Giudici P (2009) *Vinegars of the world*. Springer-Verlag, pp. 17–39. <https://doi.org/10.1007/978-88-470-0866-3>
- Wang W, Keller MD, Baughman T, Wilson BK (2020) Evaluating low-cost optical spectrometers for the detection of simulated standard and falsified medicines. *Appl Spectrosc* 74(3):323–333. <https://doi.org/10.1177/0003702819877422>
- Wu Z, Xu E, Wang F, Long J, Jiao XXA, Jin Z (2014) Rapid determination of process variables of Chinese rice wine using FT-NIR spectroscopy and efficient wavelengths selection methods. *Food Anal Methods* 6:1456–1467. <https://doi.org/10.1007/s12161-014-0021-6>
- Wulfert F, Kok WTh, Smilde AK (1998) Influence of temperature on vibrational spectra and consequences for the predictive ability of multivariate models. *Anal Chem* 70:1761–1767. <https://doi.org/10.1021/ac9709920>
- Yano T, Aimi T, Nakano Y, Tamai M (1997) Prediction of the concentrations of ethanol and acetic acid in the culture broth of a rice vinegar fermentation using near-infrared spectroscopy. *J Ferment Bioeng* 84(5):461–465. [https://doi.org/10.1016/S0922-338X\(97\)82008-9](https://doi.org/10.1016/S0922-338X(97)82008-9)
- Ye M, Yue T, Yuan Y, Li Z (2014) Application of FT-NIR spectroscopy to apple wine for rapid simultaneous determination of soluble solids content, pH, total acidity, and total ester content. *Food Bioprocess Technol* 7:3055–3062. <https://doi.org/10.1007/s11947-014-1385-8>

Publisher's Note Springer Nature remains neutral with regard to jurisdictional claims in published maps and institutional affiliations.